Earthquake Geotechnical Engineering for Protection and Development of Environment and Constructions – Silvestri & Moraci (Eds)
© 2019 Associazione Geotecnica Italiana, Rome, Italy, ISBN 978-0-367-14328-2

Framework for tracking the accumulation of shear strains during cyclic mobility

F. Humire, K. Ziotopoulou, M.S. Basson & A. Martinez
Department of Civil and Environmental Engineering, University of California, Davis, CA, USA

ABSTRACT: A framework for tracking the accumulation of shear strains in experiments exhibiting cyclic mobility behavior of liquefiable sands is implemented in order to evaluate its applicability. Shear strains are decoupled in two components: γ_0, developed at near-zero effective stress, and γ_d, developed while the soil dilates. Results show that the development of γ_d is triggered after the specimen exhibits dilative behavior, and increases up to a saturation value after liquefaction triggering. Conversely, γ_0 initiates at liquefaction triggering and its evolution per loading cycle follows an almost linear trend. These results suggest that the linear increase of post-liquefaction shear strains is related to the strains developed at near-zero effective stress, which are closely linked to the evolution of fabric at the particle scale. Further experimental work and DEM simulations are proposed to study the behavior under large deformations, and to understand the mechanism controlling strain accumulation during cyclic mobility.

1 INTRODUCTION

The evaluation of liquefaction effects on geotechnical structures requires, amongst others, the ability to estimate deformations across a range of seismic hazard levels and in-situ stress conditions. Lateral deformations developed when soils exhibit cyclic mobility behavior, wherein soil progressively accumulates shear strains after liquefaction has been triggered, can result in significant damages to structures built on or in sandy soils. On the basis of macroscopic observations of soil behavior, different constitutive models have been formulated capable of capturing the response at the element level. Still, simulation of cyclic mobility effects remains a challenging task, lacking a fundamental understanding of the mechanisms controlling the accumulation of shear strains. Evidence from Discrete Element Method (DEM) simulations, as well as from the examination of experimental data collected on sands, indicate that shear strain accumulation is controlled by particle-level mechanisms such as fabric evolution. However, the physical mechanisms controlling this phenomenon have not been fully resolved thus limiting our ability to capture it at the macroscopic level.

The present paper is part of an integrated research plan involving laboratory tests and DEM simulations, with the objective of providing information regarding the mechanisms controlling accumulation of shear strains during cyclic mobility. The first step towards taking a closer look at this behavior is to define strategies for quantitatively assessing the development of post-liquefaction shear strains. In this context, this paper focuses on the implementation of a framework for interpretation of cyclic mobility data and, in particular, for tracking the accumulation of shear strains. This is achieved by reviewing approaches available in the literature together with previous works on DEM (particularly in regard to fabric descriptors that have been shown to be closely related to the accumulation of shear strains within the cyclic mobility regime) and implementing a framework on sets of cyclic mobility data. The specific objectives of this paper are to: (1) implement a framework to study the post-liquefaction shear strain accumulation, (2) apply the framework in two laboratory undrained cyclic tests, and closely study the development of shear strains during cyclic mobility, and (3) complement the framework with insights at the particle level observed on previous works on DEM.

2 LITERATURE REVIEW

2.1 *Available frameworks for quantifying cyclic shear strain accumulation in experiments*

Shear strain accumulation in undrained cyclic experiments can at a first basis be assessed by plotting the maximum strain achieved at each loading cycle versus the number of cycles (Figure 1). This plot allows recognizing important features of experiments exhibiting cyclic mobility behavior. For example, the accumulation of shear strains per loading cycle follows an almost linear trend after initial liquefaction, as illustrated in Figure 1b. Based on this observation, Tasiopoulou et al. (unpubl.) evaluated the shear strain increment rate per loading cycle in the post-liquefaction regime for a large body of cyclic experiments, and found a dependency of this rate on the relative density, the shear stress amplitude, and the laboratory sand used in the tests.

Shamoto et al. (1997) proposed another approach for assessing the accumulation of shear strains during cyclic mobility. Based on experimental observations of undrained monotonic and cyclic torsional tests, Shamoto et al. (1997) proposed decoupling the post-liquefaction shear strains in two components: (1) a strain component developed at near-zero effective stress, denoted by γ_0, and (2) a strain component developed during dilation at non-zero effective stress, denoted by γ_d. Their results showed that γ_0 governs the development of shear strains during cyclic mobility, and suggested a dependence of γ_0 on the maximum shear strain achieved in the previous loading cycle (i.e. loading history). Later, Zhang & Wang (2012) decoupled γ_0 and γ_d for a series of undrained cyclic torsional experiments and named each strain component "fluid-like shear strain" and "solid-like shear strain", respectively. They noticed that the evolution of γ_0 versus the number of cycles follows a monotonically increasing trend. Their analysis also revealed that γ_d is almost the same for all loading cycles in the post-liquefaction regime, thus implying that γ_d depends exclusively on the current effective stress and possibly other properties of the sand.

Alternative methods for investigating cyclic mobility-related behaviors have also been presented in the literature. The development of shear strains during cyclic mobility has been captured by quantifying the shear modulus reduction at different strain levels (Zhuang et al. 2018), or by assessing the dilative tendency along the experiment (Ziotopoulou & Boulanger 2016). However, these methods are considered as being outside the scope of this paper.

2.2 *Available fabric descriptors for DEM simulations*

Particle level mechanisms, such as evolution of fabric (i.e. the spatial arrangement of solid particles, contacts, and pores in a soil matrix), control the global-scale behavior of soils (e.g. Oda et al. 1985, O'Sullivan & Cui 2009). Destructive and non-destructive techniques, such as optical microscopy, X-Ray computed tomography, and acoustic wave velocity (e.g. Wiebicke et al. 2017)

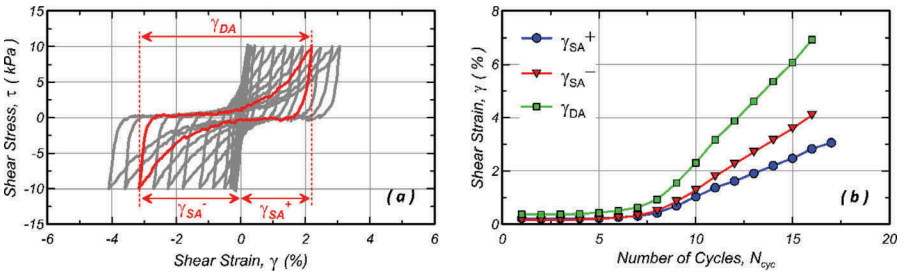

Figure 1. Results of an undrained cyclic direct simple shear test on Ottawa F-50 sand (Ziotopoulou & Morales 2018): (a) definition of single amplitude shear strains (γ_{SA}^{+} and γ_{SA}^{-}) and double amplitude shear strain (γ_{DA}), and (b) evolution of γ_{SA}^{+}, γ_{SA}^{-} and γ_{DA} per loading cycle (after Tasiopoulou et al., unpubl.).

have been employed to understand the evolution of fabric during laboratory tests. DEM codes have the additional ability of tracking micromechanical interactions between the particles of a granular assembly due to a multitude of contact-detection algorithms and the capability to model complex grain shapes and different soil gradations. This section summarizes the different fabric metrics currently available for quantifying effects related to cyclic mobility.

Contact-based descriptors are commonly used to quantify soil fabric during cyclic mobility since the number and orientation of inter-particle contacts evolve during cyclic loading. Out of these, the coordination number (C_N – mean number of contacts per particle in the assembly) has been shown via studies based on 2D and 3D DEM simulations of cyclic undrained tests to be oscillating around a value that corresponds to the minimum required to maintain a stable fabric before liquefaction triggering (e.g. Wei & Wang 2015, Wang et al. 2016).

Void-based and distance-based fabric descriptors have been introduced in recent years to describe post-liquefaction behavior. Wei et al. (2018) showed a good correlation between post-liquefaction strains and void-based metrics to define fabric anisotropy, such as the evolution of average elongation of void space (E_d) and principal direction of void space (A_d). Descriptors of the distance between particles are also appropriate to describe the cyclic mobility response. Amongst them we can find: (1) the Centroid Number (Wang & Wei 2016), which is the normalized distance between a particle centroid and the centroid of the Voronoi cell enclosing the particles, and (2) the Mean Neighboring Particle Distance ($MNPD$ – Wang et al. 2016), which is a scalar that depicts the average surface-to-surface distance between all particles and the neighboring particles needed to create a stable load-bearing structure.

3 IMPLEMENTATION ON EXPERIMENTAL DATA

3.1 *Procedure of the selected framework*

The accumulation of shear strains during cyclic mobility is assessed following the approach of Shamoto et al. (1997). The procedure to compute γ_0 and γ_d in each loading cycle is as follows:

1. Define a critical pore pressure ratio ($r_{u,crit}$) determining the limit between "solid-like" and "fluid-like" behavior;
2. Compute γ_0 as the cumulative shear strain developed with a pore pressure ratio r_u above $r_{u,crit}$. As illustrated in Figure 2, this leads to the calculation of two values of γ_0 (γ_0^+ and γ_0^-), one for each loading direction;
3. Compute γ_d as the cumulative shear strain developed during dilation with a pore pressure ratio r_u below $r_{u,crit}$ (Figure 3). In consequence, only the shear strain experienced after crossing the dilatancy (or phase transformation) line and with an increasing shear stress level is considered in γ_d. Again, two values of γ_d are computed, one for each loading direction (γ_d^+ and γ_d^-);
4. Plot the values of γ_0 and γ_d versus the number of loading cycles.

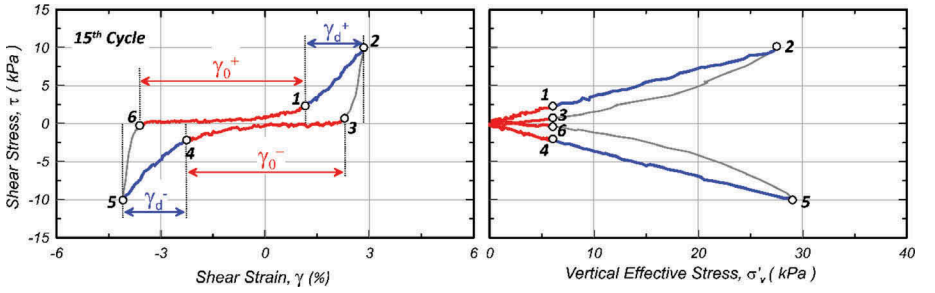

Figure 2. Near-zero effective shear strain (γ_0) and shear strain during dilation (γ_d) for the 15th loading cycle of the test illustrated in Figure 1 (modified after Tasiopoulou et al., unpubl.).

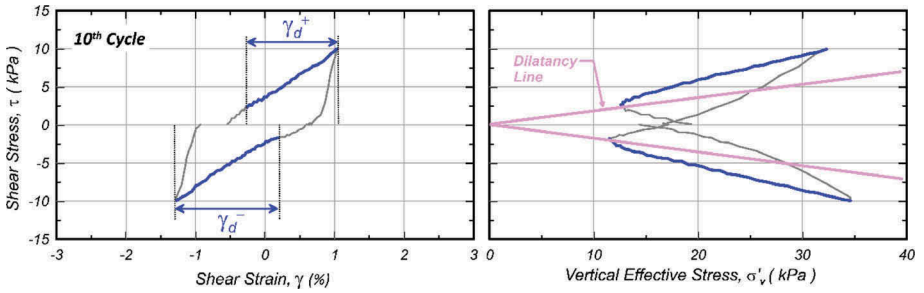

Figure 3. Estimation of γ_d before liquefaction triggering (in blue). Example for the 10th loading cycle of the test illustrated in Figure 1 using $r_{u,crit}$ = 0.95.

3.2 *Application on two undrained cyclic experiments*

The selected framework was applied on one experiment from each of the following two sets of experiment series: (1) a series of undrained cyclic direct simple shear (DSS) tests conducted on Ottawa F-50 sand at UC Davis (Ziotopoulou & Morales 2018), and (2) a series of isotropically consolidated undrained cyclic triaxial (TXC) tests conducted on Karlsruhe fine sand (Wichtmann & Triantafyllidis 2016). Relevant features of both selected experiments are summarized in Table 1. Both DSS and TXC tests demonstrated similar patterns of evolution of γ_0 and γ_d, whose values were computed considering an $r_{u,crit}$ of 0.95. Sensitivity of the results regarding the selection of $r_{u,crit}$ is discussed in Section 3.3.

3.2.1 *Direct simple shear test*

Figure 4 summarizes results obtained for the DSS experiment illustrated in Figure 1 using an $r_{u,crit}$ of 0.95. From Figure 4a, γ_d is triggered at the 5th loading cycle when the specimen starts exhibiting dilative behavior. After liquefaction triggering, γ_0 starts increasing and following an almost linear trend (Figure 4b), while γ_d tends to stabilize to a saturation value (defined as γ_d^{sat}). The evolution of γ_0 suggests that the linear increase of post-liquefaction shear strains (Figure 1b) is mostly related to the strains developed at near-zero effective stress. It is however not possible to evaluate if the rate of γ_0 decreases at higher shear strains due to limitations of the DSS device. Negligible differences are noticed between both directions of loading.

3.2.2 *Triaxial test*

Figure 5 summarizes results obtained for the triaxial test using an $r_{u,crit}$ of 0.95. In this case, $\varepsilon_{1,0}$ and $\varepsilon_{1,d}$ are defined as the "solid-like axial strain" and "fluid-like axial strain", respectively. In general, the evolution of $\varepsilon_{1,0}$ and $\varepsilon_{1,d}$ follows a similar pattern to the one observed for the DSS test. However, the saturation value of $\varepsilon_{1,d}$ (defined as $\varepsilon_{1,d}^{sat}$) obtained in extension is about 50% larger than the one obtained in compression. Since the evolutions of $\varepsilon_{1,0}$ in compression and extension are parallel to each other, the larger development of deviatoric strains in extension loading is mostly related to the development of strains during dilation.

Table 1. Summary of the experimental data.

Test	DSS	Triaxial
Relative Density, D_R (%)	63	79
Initial Effective Stress, σ'_{vo}* (kPa)	100	100
Cyclic Stress Ratio, CSR	0.10	0.25
Material	Ottawa F-50	Karlsruhe fine sand
Grain Shape	Sub-rounded	Sub-angular
Reference	Ziotopoulou & Morales (2018)	Wichtmann & Triantafyllidis (2016)

* Vertical consolidation stress for the DSS test and isotropic effective stress for the triaxial test.

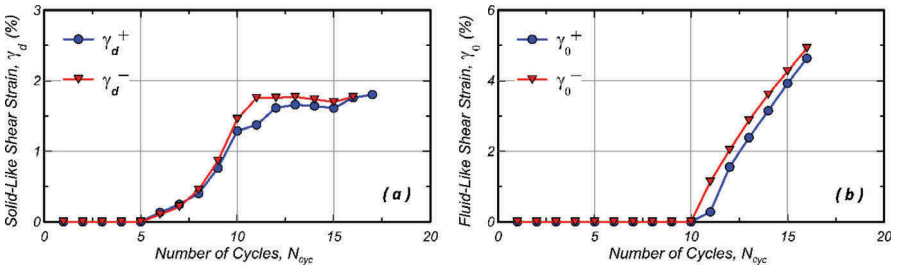

Figure 4. Shear strain accumulation for the cyclic DSS test of Ziotopoulou & Morales (2018): (a) evolution of γ_d, and (b) evolution of γ_0.

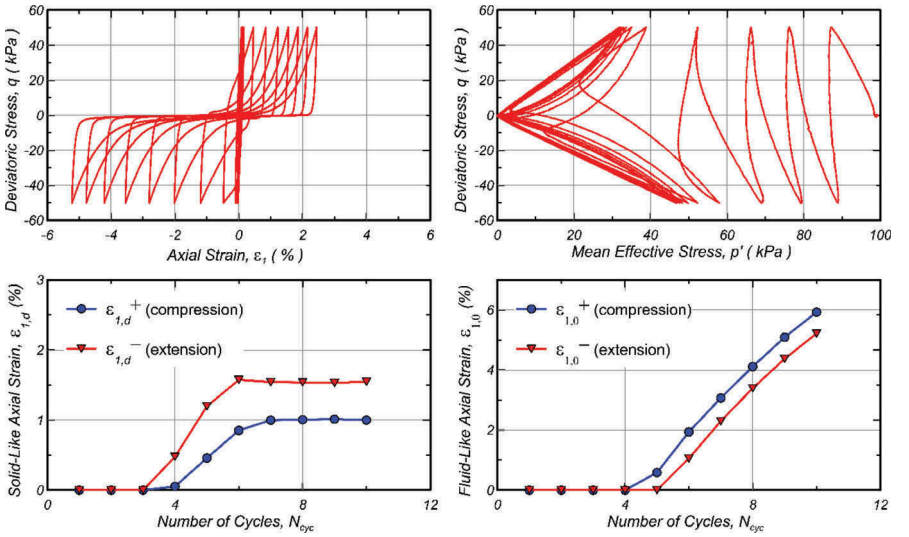

Figure 5. Evolution of $\varepsilon_{1,0}$ and $\varepsilon_{1,d}$ for the cyclic triaxial test of Wichtmann & Triantafyllidis (2016).

3.3 *Sensitivity on the selection of $r_{u,crit}$*

Selecting a transition criterion between γ_0 and γ_d is critical for the implemented framework. Herein $r_{u,crit}$ was chosen as the threshold delineating the transition from the one to the other and results showed that it is a viable criterion. However, in order to assess the sensitivity of the evolution of γ_0 and γ_d subject to this selection, the DSS experiment was re-analyzed considering four different values of $r_{u,crit}$ (Figure 6). Smaller values of γ_0 and larger values of γ_d are obtained when considering a higher $r_{u,crit}$, but the evolution patterns are very similar to each other. The main implication regarding the selection of $r_{u,crit}$ is related to the stabilization of γ_d, which is not as distinct when using a value of $r_{u,crit}$ higher than 0.95. This lack of clarity could however be attributed to the limited shear strain level achieved in the DSS experiment and, in consequence, to the few loading cycles with pore pressures above $r_{u,crit}$. Thus, although results show that pore pressure ratio can be used as the transition from solid-like to fluid-like behavior, further experimental work is required in order to reach final conclusions regarding the definition of a specific $r_{u,crit}$ and the uniqueness of this parameter as a threshold. Therefore, further experimental work is needed to fully understand the physical meaning of this transition and to define a less iterative selection of $r_{u,crit}$.

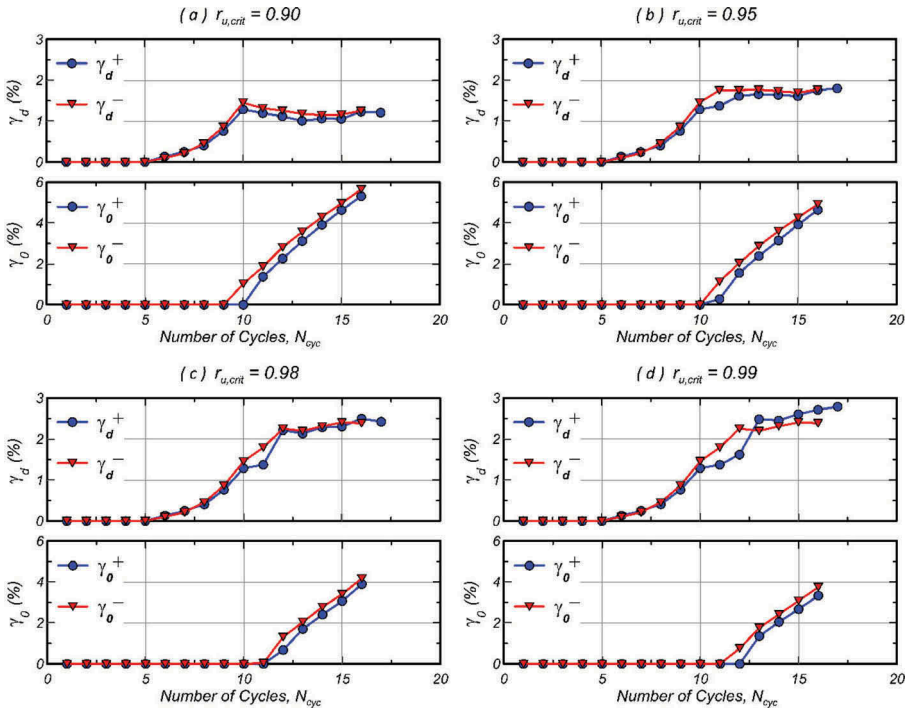

Figure 6. Evolution of γ_0 and γ_d in the DSS experiment for different values of $r_{u,\text{crit}}$: (a) $r_{u,\text{crit}}$ = 0.90, (b) $r_{u,\text{crit}}$ = 0.95, (c) $r_{u,\text{crit}}$ = 0.98, and (d) $r_{u,\text{crit}}$ = 0.99.

4 INSIGHTS FROM DEM SIMULATIONS

This section explores the relationship between shear strain accumulation and the particle level mechanisms taking place during cyclic mobility. The evolution of the fabric descriptors introduced in Section 2.2 and obtained from DEM simulations available in the literature, is compared to the evolution of γ_0 and γ_d observed in the experimental data.

The evolution of contact-based fabric descriptors was assessed using a 2D DEM simulation of an undrained cyclic test (Figure 7a) available by Wang et al. (2016). This simulation shows an overall decrease of C_N from the beginning of the cyclic loading, followed by a sudden decrease upon liquefaction triggering (Figure 7b). For the pre-liquefaction regime, the gradual increase of γ_d in the experimental data is consistent with the loss of the interparticle contacts reflected by the decreasing trend of C_N. After liquefaction triggering, the range where C_N oscillates in each loading cycle stabilizes, in such a way that γ_d develops when C_N oscillates between 2.0 and 2.7, while γ_0 when C_N oscillates between 1.1 and 2.0. Therefore, the stabilization of γ_d in the post-liquefaction regime observed in the experimental data could be explained by a stabilization of the range where C_N oscillates in each loading cycle. However, the increasing trend of γ_0 in the post-liquefaction regime cannot be explained by that stabilization. This observation is consistent with other studies (Wei & Wang 2016, 2017) that suggest fabric descriptors based on orientations of interparticle contacts are not closely related to the fluid-like behavior during cyclic mobility. Thus, contact-based metrics may not be appropriate to characterize fluid-like behavior, but they may be able to characterize the pre-liquefaction regime as well as the solid-like behavior during cyclic mobility.

A better correlation can be found between the post-liquefaction behavior and void-based and distance-based fabric descriptors. Wei et al. (2018) concluded that void-based metrics, such as E_d and A_d, evolve along with γ_0 during cyclic mobility. The same authors found a

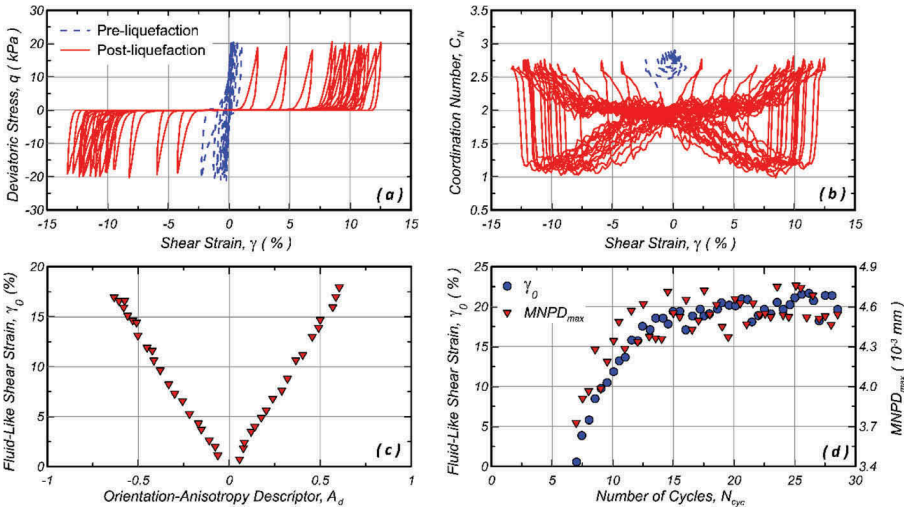

Figure 7. (a) Example of cyclic mobility 2D DEM simulation (data from Wang et al. 2016), (b) evolution of coordination number with shear strain (data from Wang, et al. 2016), (c) correlation between void orientation anisotropy, A_d, and fluid-like strain, γ_0, (after Wei et al. 2018), and (d) correlation between maximum mean neighboring particle distance $MNPD_{max}$, and γ_0 (replotted data after Wang et al. 2016).

linear relationship between A_d and γ_0 (Figure 7c), which indicates that the evolution of γ_0 in the post-liquefaction regime is associated to changes in the particle-void distribution of the grain assembly and defined a relationship between E_d and A_d (Hardening State Line) delineating regions of fluid-like and solid-like behavior. Using the distance-based descriptor $MNPD$, Wang et al. (2016) observed a relationship between γ_0 and the maximum $MNPD$ achieved in each post-liquefaction loading cycle ($MNDP_{max}$). $MNPD_{max}$ and γ_0 exhibited a similar increase in magnitude while increasing the number of loading cycles (Figure 7d). Therefore, A_d and $MNPD_{max}$ are good candidates to quantifying the fabric evolution during cyclic mobility, given the good correlation between them and γ_0.

5 CONCLUSIONS AND FUTURE WORK

Based on the approach of Shamoto et al. (1997), a framework for tracking the accumulation of post-liquefaction shear strains in laboratory tests was presented. The shear strain generated within each loading cycle is decoupled in two components: the shear strain at near-zero effective stress, denoted by γ_0, and the shear strain that occurs during dilation, denoted by γ_d. A critical pore pressure ratio $r_{u,crit}$ is considered as the limit between γ_0 and γ_d. The framework was successfully applied in two undrained cyclic experiments (direct simple shear and triaxial tests). According to the analysis results, γ_d is triggered when the specimen starts exhibiting dilative behavior, and monotonically increases until it reaches a saturation value (γ_d^{sat}) at liquefaction triggering or few cycles after that. On the other hand, γ_0 initiates at liquefaction triggering and its evolution per loading cycle follows an almost linear trend. These results suggest that the linear increase of post-liquefaction shear strains is mostly related to shear strains developed at near-zero effective stress. Further experimental work is needed to elucidate if γ_0 decreases or arrests at higher strain levels.

The sensitivity of the results to the selection of $r_{u,crit}$ was investigated. It was found that the values of γ_0 and γ_d depend on the selected $r_{u,crit}$, but their overall evolutions follow similar patterns independently of the selected $r_{u,crit}$. The main implication regarding the selection of $r_{u,crit}$

is that the stabilization of γ_d is not as clear when using a higher value of $r_{u,crit}$, which is probably related to the limited shear strain level achieved in the experiment.

The evolution of different fabric descriptors in previous DEM works was compared to the evolution of γ_0 and γ_d observed in the experimental data. Despite contact-based descriptors being the most straightforward to work with, they provide limited information during the post-liquefaction stage. For example, the coordination number shows no correlation with the accumulation of γ_0 during cyclic mobility. Conversely, void-based and distance-based descriptors, such as A_d and $MNPD_{max}$, seem to have better relationship with post-liquefaction shear strains.

The implemented framework and the associated fabric-based descriptors were shown to be promising, however further experimental work and DEM simulations are proposed to study the cyclic mobility behavior at large deformations. More specifically, future work will focus on: (1) investigating the possibility of achieving a saturation value for γ_0 at large strain levels, (2) evaluating the factors influencing the evolution of γ_0 and γ_d, and (3) elucidating the relationship between the particle level response and the development of γ_0 and γ_d. Results of this work are expected to provide insights regarding the fundamental mechanism controlling the post-liquefaction shear strain accumulation towards future improvements in constitutive models for liquefaction analysis.

The proposed framework will be applied in undrained cyclic DSS tests to be performed at UC Davis in a recently acquired device able to achieve large shear strain levels (γ_{SA} up to 10%). The testing plan considers experiments on sands with different particle properties (e.g. grain shape, mean grain size, gradation) and subjected to different loading conditions (e.g. sloping-ground conditions, non-uniform cyclic loading). These experiments will allow the study of the evolution of γ_0 and γ_d at large strain levels, and to explore correlations of γ_d^{sat} and the rate of γ_0 per loading cycle with relative density, loading conditions, and grain properties. Also, 3D cyclic undrained DSS tests will be simulated using DEM to develop further understanding of the evolution of different fabric descriptors with the accumulation of fluid-like and solid-like strains.

REFERENCES

Oda, M., Nemat-Nasser, S. & Konishi, J. 1985. Stress-induced anisotropy in granular masses. *Soils and Foundations* 25(3): 85–97.

O'Sullivan, C. & Cui, L. 2009. Micromechanics of granular material response during load reversals: Combined DEM and experimental study. *Powered Technology* 139: 289–302.

Shamoto, Y., Zhang, J.-M. & Goto, S. 1997. Mechanism of large post-liquefaction deformation in saturated sand. *Soils and Foundations* 37(2): 71–80.

Tasiopoulou, P., Ziotopoulou, K., Humire, F., Giannakou, A., Chacko, J. & Travasarou, T. 2019. Development and implementation of a semi- empirical framework for modeling post-liquefaction deformation accumulation of sands. *J Geotech and Geoenv Eng* (*under review*).

Thornton, C. 2000. Numerical simulations of deviatoric shear deformation of granular media. *Géotechnique* 50(1): 43–53.

Wang, G. & Wei, J. 2016. Microstructure evolution of granular soils in cyclic mobility and post-liquefaction process. *Granular Matter* 18(3): 51.

Wang, R., Fu, P., Zhang, J.-M. & Dafalias, Y. F. 2016. DEM study of fabric features governing undrained post-liquefaction shear deformation of sand. *Acta Geotechnica* 11(6): 1321–1337.

Wei, J. & Wang, G. 2015. Microstructure evolution of granular soils during liquefaction process. In Kenichi Soga (ed.). *Proc. Intern. symp. on Geomechanics from Micro to Macro, Cambridge 1-3 September 2014*.

Wei, J. & Wang, G. 2017. Discrete-element method analysis of initial fabric effects on pre- and post-liquefaction behavior of sands. *Géotechnique Letters* 7(2): 61–166.

Wei, J., Huang, D. & Wang, G. 2018. Microscale descriptors for particle-void distribution and jamming transition in pre- and post-liquefaction of granular soils. *J of Eng Mechanics* 144(8): 4018067.

Wichtmann, T. & Triantafyllidis, T. 2016. An experimental database for the development, calibration and verification of constitutive models for sand with focus to cyclic loading: Part I - tests with monotonic loading and stress cycles. *Acta Geotechnica* 11(4): 739–761.

Wiebicke, M., Andò, E., Herle, I. & Viggiani, G. 2017. On the metrology of interparticle contacts in sand from x-ray tomography images. *Measurement Science and Technology* 28(12): 124007.
Zhang, J.-M. & Wang, G. 2012. Large post-liquefaction deformation of sand, part I: Physical mechanism, constitutive description and numerical algorithm. *Acta Geotechnica* 7(2): 69–113.
Zhuang, H., Wang, R., Chen, G., Miao, Y. & Zhao, K. 2018. Shear modulus reduction of saturated sand under large liquefaction-induced deformation in cyclic torsional shear tests. *Eng Geology* 240: 110–122.
Ziotopoulou, K. & Boulanger, R. W. 2016. Plasticity modeling of liquefaction effects under sloping ground and irregular cyclic loading conditions. *Soil Dynamics and Earthquake Engineering* 84: 269–283.
Ziotopoulou, K. & Morales, B. 2018. Direct simple testing of Ottawa F-50 sand. *Soil Interactions Laboratory Data Report*.